An adjustable, high sensitivity, wide dynamic range two channel wave-front sensor based on moiré deflectometry

Saifollah Rasouli,[1,2,*] **M. Dashti,**[1] **and Anamparambu. N. Ramaprakash**[3]

[1]*Department of Physics, Institute for Advanced Studies in Basic Sciences (IASBS), Zanjan 45137-66731, Iran*

[2]*Optics Research Center, Institute for Advanced Studies in Basic Sciences (IASBS), Zanjan 45137-66731, Iran*

[3]*Inter-University Centre for Astronomy and Astrophysics, Post Bag 4, Ganeshkhind, Pune - 411 007, India*

[*]*rasouli@iasbs.ac.ir*

Abstract: An adjustable, high sensitivity, wide dynamic range two channel wave-front sensor based on moiré deflectometry has been constructed for measuring distortions of light wave-front transmitted through the atmosphere. In this approach, a slightly divergent laser beam is passed through the turbulent ground level atmosphere and then a beam-splitter divides it into two beams. The beams pass through a pair of moiré deflectometers which are installed parallel and close together. From deviations in the moiré fringes we calculate the two orthogonal components of angle of arrival at each location across the wave-front. The deviations have been deduced in successive frames which allows evolution of the wave-front shape to be determined. The dynamic range and sensitivity of detection are adjustable by merely changing the separation of the gratings and the angle between the rulings of the gratings in both of channels. The spatial resolution of the method is also adjustable by means of bright, dark, and virtual traces for given moiré fringes without paying a toll in the measurement precision.

OCIS codes: (010.7350) Wave-front sensing; (110.6760) Talbot effect; (120.4120) Moiré techniques; (010.1330) Atmospheric turbulence.

References and links

1. M. Lombardo, and G. Lombardo, "New methods and techniques for sensing the wave aberrations of human eyes," Clin. Exp. Optom. **92**, 176–186 (2009).
2. F. Roddier, *Adaptive optics in astronomy* (Cambridge university press, Cambridge, United Kingdom) (1999).
3. R. V. Shack, and B. C. Platt, "Production and use of a lenticular Hartmann screen," J. Opt. Soc. Am. **61**, 656 (1971).
4. B. C. Platt, R. Shack, "History and principles of Shack-Hartmann wavefront sensing," J. Refract. Surg. **17**, S573–S577 (2001).
5. E. Roddier, "Curvature sensing and compensation: a new concept in adaptive optics," Appl. Opt. **27**, 1223–1225 (1988).
6. G. W. R. Leibbrandt, G. Harbers, and P. J. Kunst, "Wavefront analysis with high accuracy by use of a double-grating lateral shearing interferometer," Appl. Opt. **35**, 6151–6161 (1996).
7. R. A. Gonsalves, "Phase retrieval and diversity in adaptive optics," Opt. Eng. **21**, 829–832 (1982).
8. R. Ragazzoni, and J. Farinato, "Sensitivity of a pyramidic wave front sensor in closed loop adaptive optics," Astron. Astrophys. **350**, L23–L26 (1999).

#128934 - $15.00 USD Received 24 May 2010; revised 8 Jul 2010; accepted 7 Sep 2010; published 29 Oct 2010

9. R. Legarda-Saenz, "Robust wavefront estimation using multiple directional derivatives in moiré deflectometry," Opt. Lasers Eng. **45**, 915–921 (2007).
10. J. A. Quiroga, D. Crespo, and E. Bernabeu, "Fourier transform method for automatic processing of moiré deflectograms," Opt. Eng. **38**, 974–982 (1999).
11. N. H. Salama, D. Patrignani, L. D. Pasquale, and E. E. Sicre, "Wavefront sensor using the Talbot effect," Opt. Laser Technol. **31**, 269–272 (1999).
12. Ch. Siegel, F. Loewenthal, and L. E. Balmer, "A wavefront sensor based on the fractional Talbot effect," Opt. Commun. **194**, 265–275 (2001).
13. R. Sekine, T. Shibuya, K. Ukai, S. Komatsu, M. Hattori, T. Mihashi, N. Nakazawa, and Y. Hirohara, "Measurement of wavefront aberration of human eye using Talbot image of two-dimensional grating," Opt. Rev. **13**, 207–211 (2006).
14. M. Rottenkolber, and H. Podbielska, "Measuring ophthalmologic surfaces by means of moiré deflectometry," Opt. Eng. **35**, 1124–1133 (1996).
15. S. Rasouli, "Use of a moiré deflectometer on a telescope for atmospheric turbulence measurements," Opt. Lett. **35**, 1470–1472 (2010); and references 1-4 therein.
16. S. Rasouli, Anamparambu N. Ramaprakash, H. K. Das, C. V. Rajarshi, Y. Rajabi, and M. Dashti, "Two channel wavefront sensor arrangement employing moiré deflectometry," in *Optics in Atmospheric Propagation and Adaptive Systems XII*, A. Kohnle, K. Stein, and J. D. Gonglewski, ed., Proc. SPIE **7476**, 74760K-1–9 (2009).
17. S. Rasouli, and M. T. Tavassoly, "Application of the moiré deflectometry on divergent laser beam to the measurement of the angle of arrival fluctuations and the refractive index structure constant in the turbulent atmosphere," Opt. Lett. **33**, 980–982 (2008).
18. J. Herrmann, "Least-squares wave front errors of minimum norm," J. Opt. Soc. Am. **70**, 28–35 (1980).
19. B. R. Hunt, "Matrix formulation of the reconstruction of phase values from phase differences," J. Opt. Soc. Am. **69**, 393–399 (1979).

1. Introduction

Various wave-front sensing techniques have been developed for use in a variety of applications ranging from measuring the wave aberrations of human eyes [1] to adaptive optics in astronomy [2]. The most commonly used wave-front sensors are the Shack-Hartmann [3,4], curvature sensing [5], shearing interferometry [6], phase retrieval methods [7] and Pyramid wave-front sensor [8]. The Shack-Hartmann sensor is also the most commonly used technique for measurement of turbulence-induced phase distortions for various applications in atmospheric studies and adaptive optics. But, the dynamic range of the Shack-Hartmann sensor is limited by the optical parameters of its microlenses, namely, the spacing and the focal length of the microlens array.

Although not so well known, Talbot effect and moiré deflectometry have been employed for wave-front sensing in different fields and in several different ways [9–13]. For example, a technique for aspheric surface metrology by means of dual-path moiré deflectometry has been suggested by [14]. The method used by them is based on measurements of the distribution of deflection angles for a line near the center of the moiré deflectometer. A limitation of the set-up is that the method is applicable only for stationary cases. To the best of our knowledge, moiré deflectometry has not been used for sensing time-varying distortions of wave-fronts, although by means of moiré technique we have estimated atmospheric turbulence parameters in various schemes [15]. Based on the above experience, we recently suggested a two channel wave-front sensor based on moiré deflectometry [16]. However, it was recognized that the implementation of the method is not very straightforward. In this paper we present a new, reliable, and quite simple method for wave-front sensing. Also, using an algorithm developed for moiré fringe processing, the spatial resolution of the method is improved. In this paper, the theory of the approach by means of which angle of arrival (AA) fluctuations across the wave-front can be determined is presented.

A schematic diagram of the experimental setup is shown in Fig. 1. A slightly divergent laser beam passes through a turbulent ground level atmosphere and enters the wave-front sensor. Then a beam splitter splits it into two beams, a mirror reflects the second beam into a direction

#128934 - $15.00 USD Received 24 May 2010; revised 8 Jul 2010; accepted 7 Sep 2010; published 29 Oct 2010

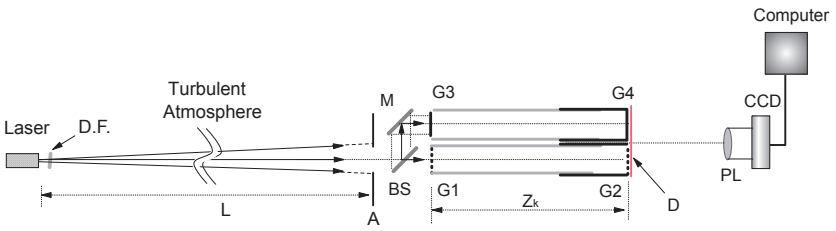

Fig. 1. Schematic diagram of the experimental setup. DF, A, BS, M, Z_k, D, PL stand for the neutral density filter, square aperture, beam splitter, mirror, Talbot distance, diffuser, and projecting lens, respectively. G1, G2, G3 and G4 stand for the gratings.

parallel to the first beam's propagation direction, and the two beams pass through a pair of moiré deflectometers. The moiré deflectometers are installed quite close to each other. Directions of the gratings' rulings are almost parallel in each moiré deflectometer but are perpendicular in the two beams. Moiré patterns are formed at a plane where the second gratings of the moiré deflectometers and a diffuser are installed. The moiré patterns from both the beams are projected on a CCD camera. Successive moiré patterns are recorded by the CCD camera and transferred to a computer, to allow temporal fluctuations of the wave-front phase to be measured highly accurately. Displacements of the moiré fringes in the recorded patterns correspond to the fluctuations of two orthogonal components of the AA across the wave-front. The fluctuations have been deduced in successive frames, and the evolution of the wave-front shape is determined.

2. Theoretical framework

In a usual configuration of moiré deflectometer consisting of two Ronchi gratings, the set up is sensitive to the incoming wave-front changes only in one direction normal to its rulings. In this work, we have used two moiré deflectometers in two channels. We choose a coordinate system so that in the first channel the grating rulings are in the x-direction and those in the second channel are in the y-direction, as shown in Fig. 1. Theoretical considerations are similar for both channels. We present the theory for determining the AA fluctuations for a single channel first. Later the information from both channels are combined.

We assume that the wave-front illuminates two gratings G1 and G2 of equal periods d, separated by Z_k along the optical axis, where Z_k is the kth Talbot distance of the first grating. Due to wave-front distortions, the self-image of the first grating fluctuates on the second grating. The changes in the moiré patterns are related to grating separation in the experimental setup Z_k, the relative rotation between the grating rulings $\theta = \frac{d}{d_m}$ in the moiré deflectometer, and the y component of the AA fluctuations of the incident wave-front $\alpha_y(x,y)$. According to moiré formulation, for displacement $\delta y(x,y)$ of the self-image in a direction normal to the grating rulings, moiré fringes are shifted by $\delta x_m(x,y)$ given by

$$\delta x_m(x,y) = \frac{d_m}{d}\delta y(x,y), \tag{1}$$

where d_m is the moiré fringe spacing. Recalling that when the self-image of the first grating on the second grating is displaced by l the AA changes by $\alpha = l/Z_k$, the component $\alpha_y(x,y)$ of the AA fluctuation in the direction perpendicular to the grating rulings (parallel to the moiré trace) on the first grating is given by

$$\alpha_y(x,y) = \frac{\delta y(x,y)}{Z_k} = \frac{1}{Z_k}\frac{d}{d_m}\delta x_m(x,y). \tag{2}$$

#128934 - $15.00 USD Received 24 May 2010; revised 8 Jul 2010; accepted 7 Sep 2010; published 29 Oct 2010

According to Eq. (2), by increasing the distance between the gratings, increasing the moiré fringe spacing, or decreasing the period of the gratings, the measurement precision of AA fluctuations can be improved. In this work, we have used $d = \frac{1}{15}$ mm, and Z_k=22.4 cm, and by using $\frac{\delta x_m(x,y)}{d_m} = \frac{1}{50}$, the minimum measurable AA fluctuations, is determined to be 5.9×10^{-6} rad or 1.2 arc sec. The minimum measurable value of $\frac{\delta x_m(x,y)}{d_m}$ is influenced by the number of CCD pixels which were covered by the moiré fringe spacing. On the other hand, if we stipulate that the maximum measurable displacement of a trace is equal to half the moiré fringe spacing, one can measure AA fluctuations in the range -30 to +30 arc sec without having any adjustment in the set-up.

Now, we can generalize the formulation for the second channel. The component $\alpha_x(x,y)$ of the AA fluctuation in the direction perpendicular to the rulings of gratings G3 and G4 (parallel to the corresponding moiré traces) on the G3 grating is given by:

$$\alpha_x(x,y) = \frac{\delta x(x,y)}{Z_k} = \frac{1}{Z_k}\frac{d}{d_m'}\delta y_m(x,y), \tag{3}$$

where d_m' is the moiré fringe spacing in the second channel. Thus, we can get

$$[\alpha_x(x,y), \alpha_y(x,y)] = \frac{d}{Z_k}\left[\frac{\delta y_m(x,y)}{d_m'}, \frac{\delta x_m(x,y)}{d_m}\right]. \tag{4}$$

Since $\alpha_x(x,y)$ and $\alpha_y(x,y)$ are equal to the incident wave-front gradients in x and y-directions, respectively, the incident wave-front gradients at a point (x,y) are determined by

$$\left[\frac{\partial U(x,y)}{\partial x}, \frac{\partial U(x,y)}{\partial y}\right] = \frac{d}{Z_k}\left[\frac{\delta y_m(x,y)}{d_m'}, \frac{\delta x_m(x,y)}{d_m}\right]. \tag{5}$$

It should be mentioned that, the presented formulation is valid for a collimated incoming laser beam. In principal, for a divergent incoming laser beam some modifications are needed [17]. In this work, we have used L=360 m, $d = \frac{1}{15}$ mm, and Z_k=22.4 cm, and by using Eqs. (2) and (4) of [17], the moiré fringe spacing, is determined to be 10.6 cm when the relative rotation between the grating rulings, θ, is equal to zero. This is several times larger than the size of the gratings that we have used. As a result the beam divergence in the incoming laser beam is not important and the above simple formulation is applicable.

3. Moiré fringes processing

In the previous work [16], we used only the displacements of the bright moiré fringes for evaluation of the wave-front shape, as it is the most commonly employed approach. According to Eq. (4), by increasing the moiré fringe spacing the precision of AA fluctuations measurements can be improved. But, then the number of moiré fringes in the field of view as well as the spatial resolution of the method is decreased. In this paper we have used an improved algorithm for processing the moiré fringes to overcome this limitation. Here we have introduced a new concept that we call virtual traces in the moiré patterns. In this approach, the traces of bright moiré fringes, dark moiré fringes, and of points with intensities equal to the mean intensity of the adjacent bright and dark traces (first order virtual traces) were determined. One can potentially produce a large number of virtual traces between two adjacent bright and dark traces by using their intensities and locations. According to Eqs. (4) and (5) the displacements of the traces in the recorded patterns with respect to their reference positions correspond to the fluctuations of AA components which in turn represent the local wave-front gradients. With our approach proposed here, the precision of AA fluctuations can be improved by increasing the moiré fringe

#128934 - $15.00 USD Received 24 May 2010; revised 8 Jul 2010; accepted 7 Sep 2010; published 29 Oct 2010

spacing (by merely changing the separation of the gratings and/or the angle between the rulings of the gratings in both of moiré deflectometers), while at the same time the desired spatial resolution can be achieved by using a number of virtual traces. Finally one can use the concept of virtual traces in all of the moiré based methods for atmospheric turbulence measurements [15] to improve their spatial resolution.

4. Wave-front reconstruction

Another important part of a wave-front sensor is the software to convert the 2-D wave-front gradient data into 2-D wave-front phase data. In order to perform the wave-front reconstruction from the measured moiré patterns, we consider the displacements of the bright, dark, and the first order virtual traces with respect to their reference positions, which represents an estimate of the local *x*-gradients or *y*-gradients of the wave-front phase. The reference positions of the traces are determined from a long-exposure frame. In practice, by considering two sets of vertical and horizontal moiré traces of a frame in a *x*-*y* coordinate system (the vertical and horizontal traces are overlapped in the *x*-*y* coordinate system), the intersection points of the vertical and horizontal bright, dark, and the first order virtual traces are determined. *x*-gradients and *y*-gradients of the wave-front are deduced from the displacements of the intersection points in successive frames. From this 2-D gradient field we performed an estimate of the wave-front.

5. Experimental results

In the experiment, a He-Ne laser beam propagates through a turbulent surface layer of the atmosphere and passes through a square aperture with the dimension 20 $mm \times 20$ mm, and then enters the wave-front sensor (Fig. 1). The source and the experimental set-up are installed at a height of 55 cm, over an asphalted area, at a distance 360 m from each other. Within the wave-front sensor, the laser beam splits into two beams by an amplitude beam splitter. The second beam is reflected by a mirror, M, to a direction parallel to the first beam propagation direction. The beams strike the first gratings G1 and G3, respectively. The gratings G1 and G3 are installed on a single holder and the second gratings G2 and G4 are installed on another holder. The holders are installed on an optical rail of changeable length to choose the desired Talbot's distance. The grating holders are held on rotary mounts which can rotate about the optical axis for adjustment of the angle between the grating rulings. In the experiment G2 and G4 are installed at a distance of 22.4 cm from G1 and G3 respectively. All the gratings are identical and have a ruling period of $\frac{1}{15}$ mm. Moiré patterns are formed on a plane where the G2 and G4 and a diffuser, D, are installed. Using a projection lens, PL, both of the moiré patterns are projected on a CCD camera. After alignment of the setup, the beam intensity was reduced by a neutral density filter to a level below the saturation level of the CCD. The moiré fringes were recorded at a sampling rate of 60 frames/s with the CCD camera (model DMK 21AU), and fed to the PC. In the described experiment, the digitized frames consist of 480×640 pixels. Moiré pattern in each channel consists of about 276×276 pixels and d_m was covered by 40 pixels in both of channels. The measurement precision of AA fluctuations was about 1.5 arc sec in the x and y directions. Several sets of experimental data were recorded and digitized. Each set of data was collected in 5sec and contained 300 frames. The experiment was performed at IASBS. A typical recorded frame is shown in Fig. 2. Each frame consists of two sets of orthogonal moiré patterns. The low frequency illumination of the pattern of the fringes were recovered by using a spatial fast Fourier transform.

Once all 300 data frames of the data set were processed, the traces of bright and dark moiré fringes, the first order virtual traces, and the mean position of the traces (the reference positions of the traces) were determined to within one pixel accuracy. In Fig. 3 (a) and (d) typical moiré fringes in the horizontal and vertical directions are shown. In Fig. 3 (b) and (e) the correspond-

#128934 - $15.00 USD Received 24 May 2010; revised 8 Jul 2010; accepted 7 Sep 2010; published 29 Oct 2010

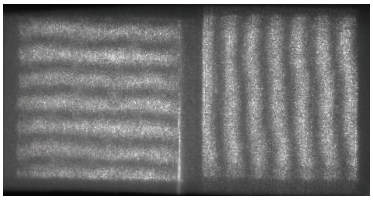

Fig. 2. A typical recorded frame consists of two sets of orthogonal moiré patterns.

ing low-frequency illumination of the patterns are shown. Derived traces of bright and dark moiré fringes and the first order virtual traces are shown in 3 (c) and (f). The background movie (Media 1) of Fig. 3, contains all of the recorded patterns and the corresponding bright, dark, and first order virtual traces.

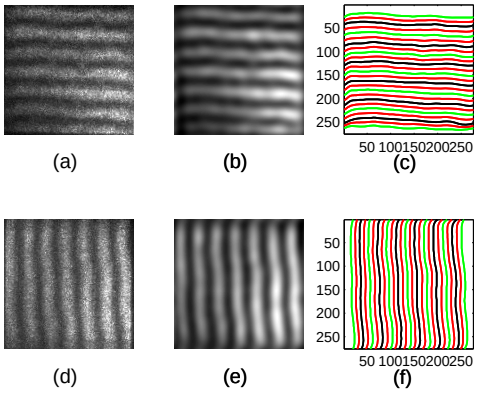

Fig. 3. (Color online) (a) and (d) typical moiré fringes in the horizontal and vertical directions, (b) and (e) the corresponding low-frequency illumination of the patterns. The corresponding bright and dark moiré fringes traces and the first order virtual traces are shown in (c) and (f). All the recorded frames, the corresponding low-frequency illumination and traces can be observed in the background "movie" (Media 1 MPEG, 4.2 MB).

For all the bright, dark and the first order virtual traces of the moiré fringes in Fig. 2, the intersection points are determined. Displacement vectors of the intersection points with respect to their mean positions are calculated and are shown in Fig. 4. A larger shift is visualized by a larger length of the arrow. From the magnitude of the displacements in x and y directions and using Eqs. (4) and (5) the wave-front gradients in the corresponding directions were obtained. The background movie (Media 2) of Fig. 4, contains the displacement vectors of all of the intersection points for 300 successive frames. In the described experiment, in order to perform the wave-front reconstruction from the measured wave-front slopes, we have used Hudgin's discretization [18, 19]. The reconstructed wave-front surface plot, corresponding to distortions generated by atmospheric turbulence are shown in Fig. 5. The background movie (Media 3) of Fig. 5, shows the evolution of wave-front in 300 successive frames. Let us now consider the temporal and spatial evolution of the wave-front in the background movie (Media 3) of Fig. 5. A good fit to all of the reconstructed wave-front surfaces over the area 20×20 mm^2 is almost a plane wave. As a result, the major atmospheric distortions over the selected area are tip and tilt.

#128934 - $15.00 USD Received 24 May 2010; revised 8 Jul 2010; accepted 7 Sep 2010; published 29 Oct 2010

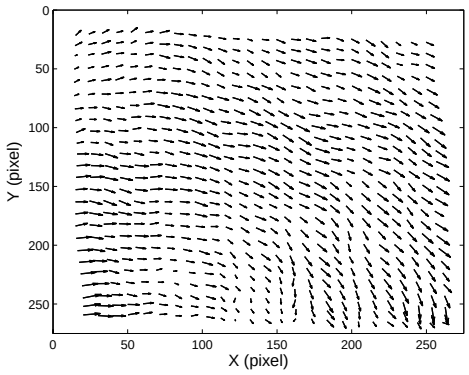

Fig. 4. Displacement vectors of intersection points of all the traces. A larger shift is visualized by a larger length of the arrow. The "movie" (Media 2) shows the corresponding patterns for all of the successive recorded frames (MPEG, 12.2 MB).

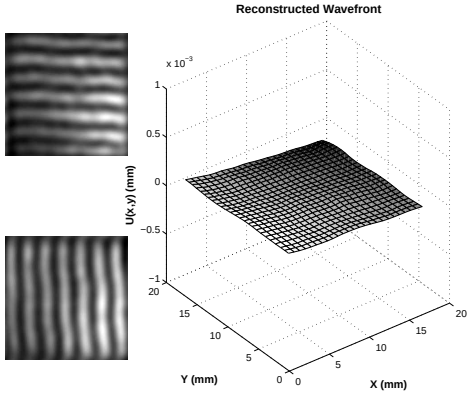

Fig. 5. Moiré fringes in the horizontal and vertical directions and the reconstructed wavefront, surface plot, corresponding to the distortions induced by atmospheric turbulence. The corresponding "movie" (Media 3) for all of the successive recorded frames can be observed in the background (MPEG, 3.4 MB).

#128934 - $15.00 USD Received 24 May 2010; revised 8 Jul 2010; accepted 7 Sep 2010; published 29 Oct 2010

Thus, it is easy to say that Fried's parameter is larger than the size of the beam size entering the wave-front sensor. Also, considering the temporal evolution of the reconstructed wave-front, it is clear that the atmospheric distortions are changing faster than our frame sampling rate. By some changes in the set-up, for example increasing the size of the gratings and the size of the beam splitter to cover a large area of the wave-front and using a high speed CCD camera, one can investigate more precisely the effect of the atmospheric turbulence. By employing the mentioned modification to the wave-front sensor, the atmospheric turbulence parameters can be determined more precisely. This work is in progress and will be published in the future.

6. Conclusion

In this paper we have presented an adjustable, high-sensitivity, wide dynamic range two channel wave-front sensor based on moiré deflectometry. We have also developed software for analyzing the moiré fringes by introducing the concept of virtual traces. In the proposed wave-front sensor the dynamic range and sensitivity of detection are adjustable by merely changing the separation of the gratings and the angle between the rulings of the gratings in both the moiré deflectometers. The spatial resolution of the method is also adjustable by means of bright, dark, and virtual traces for a given set of moiré fringes without paying a toll in the measurement precision. The implementation of the technique is straightforward. Compared to our previously proposed two channel wave-front sensor, this method is reliable and quite simple. The measurement is relatively insensitive to the alignment of the beam into the sensor. This sensor has many practical applications ranging from wave aberrations of human eyes to adaptive optics in astronomy. For low light applications as one would normally expect in astronomy, high sensitive detectors are required. Also, to reduce the energy loss, moiré deflectometers can be performed with phase gratings.

Acknowledgments

S. Rasouli would like to acknowledge Professor Yousef Sobouti for his valuable support for accomplishing the research described in this paper. Also S. Rasouli gratefully acknowledge partial support by the Institute for Advanced Studies in Basic Sciences (IASBS) Research Council under grant No. G2009IASBS107.

#128934 - $15.00 USD Received 24 May 2010; revised 8 Jul 2010; accepted 7 Sep 2010; published 29 Oct 2010

#128934 - $15.00 USD Received 24 May 2010; revised 8 Jul 2010; accepted 7 Sep 2010; published 29 Oct 2010

#128934 - $15.00 USD Received 24 May 2010; revised 8 Jul 2010; accepted 7 Sep 2010; published 29 Oct 2010